Plasma-enhanced chemical vapor deposition of boron nitride thin films from $B_2H_6-H_2-NH_3$ and $B_2H_6-N_2$ gas mixtures

J. L. Andújar,[a] E. Bertran, and M. C. Polo
Departament de Física Aplicada i Electrònica, Universitat de Barcelona, Avinguda Diagonal 647, E-08028 Barcelona, Spain

(Received 17 July 1997; accepted 21 November 1997)

Highly transparent and stoichiometric boron nitride (BN) films were deposited on both electrodes (anode and cathode) of a radio-frequency parallel-plate plasma reactor by the glow discharge decomposition of two gas mixtures: $B_2H_6-H_2-NH_3$ and $B_2H_6-N_2$. The chemical, optical, and structural properties of the films, as well as their stability under long exposition to humid atmosphere, were analyzed by x-ray photoelectron, infrared, and Raman spectroscopies; scanning and transmission electron microscopies; and optical transmittance spectrophotometry. It was found that the BN films grown on the anode using the $B_2H_6-H_2-NH_3$ mixture were smooth, dense, adhered well to substrates, and had a textured hexagonal structure with the basal planes perpendicular to the film surface. These films were chemically stable to moisture, even after an exposition period of two years. In contrast, the films grown on the anode from the $B_2H_6-N_2$ mixture showed tensile stress failure and were very unstable in the presence of moisture. However, the films grown on the cathode from $B_2H_6-H_2-NH_3$ gases suffered from compressive stress failure on exposure to air; whereas with $B_2H_6-N_2$ gases, adherent and stable cathodic BN films were obtained with the same crystallographic texture as anodic films prepared from the $B_2H_6-H_2-NH_3$ mixture. These results are discussed in terms of the origin of film stress,the effects of ion bombardment on the growing films, and the surface chemical effects of hydrogen atoms present in the gas discharge.
 [S0734-2101(98)02302-1]

I. INTRODUCTION

Thin films of boron nitride (BN) have recently attracted a lot of interest due to the combination of properties offered by this nonoxide ceramic material, such as low density, optical transparency, hardness, chemical inertness, high electrical resistivity, and high thermal conductivity.[1] BN has several crystalline structures similar to the structures in carbon. Cubic BN (*c*-BN), analogous to diamond, is extremely hard and more stable than diamond at high temperatures.[2] Hexagonal BN (*h*-BN) has a layered structure similar to graphite, but is a transparent, very refractory corrosion-resistant material with good dielectric properties.[3] In addition, disordered turbostratic modifications of *h*-BN, which range from perfectly oriented *h*-BN to completely disordered amorphous BN (*a*-BN), are commonly found in BN films.

BN coatings have been successfully used in high-temperature crucibles, masks for x-ray lithography, heat sinks, and sodium barriers in microelectronics.[4] Newer applications of BN films include their use in microelectronic devices, not only as passivation layers but also as active dielectric layers,[5] as well as wear and corrosion-protective coatings for cutting tools and optical windows.[6]

Excellent reports on the preparation of BN films by low-pressure physical vapor deposition (PVD) and chemical vapor deposition (CVD) processes can be found in the recent literature.[2–4,6,7] Most successful methods for the preparation of films containing some amount of *c*-BN are based on ion-assisted PVD techniques, such as ion-assisted evaporation[8] and bias sputtering,[9] because the ion bombardment during film growth is considered an essential condition for obtaining *c*-BN. Nevertheless, the high compressive stress caused by ion bombardment generally leads to poor adhesion and often to delamination of the films.[10] However, uniform high-purity noncubic BN coatings on irregularly shaped surfaces can be obtained with CVD methods. Several gas sources have been used, the most common being BCl_3-NH_3, BF_3-NH_3, and $B_2H_6-NH_3$.[3] Borazine ($B_3N_3H_6$) and organometallic precursors have also been employed. Thermal CVD of BN is usually performed at processing temperatures of about 1000 °C, which is a limiting factor for many uses. Nevertheless, the lower temperatures involved in plasma-enhanced CVD (PECVD) processes, typically, in the 200–300 °C range, allow a great variety of substrates used in the semiconductor and metallurgical industries to be BN coated. With capacitively coupled radio-frequency (rf) discharges, by far the most widely used plasma source for low-pressure materials processing, noncubic BN films are usually obtained.[11–15] PECVD films with some fraction of the *c*-BN phase have been obtained using higher-density plasma sources such as magnetic-field-enhanced rf glow discharges,[16] inductively coupled rf discharges,[17] and electron cyclotron resonance plasmas.[18]

Owing to the complexity of the PECVD processes, the properties of the films are strongly dependent on the particular deposition system and the gas chemistry used. Therefore, the optimized conditions found in a given system cannot generally be extrapolated to another. Further, in capacitive rf discharges, the location of substrates on the grounded elec-

[a]Electronic mail: jandujar@electra.fae.ub.es

trode (anode) or on the powered electrode (cathode) greatly affects the structure and properties of deposited films, since, as a result of the negative self-bias voltage developed in the cathode, the impact energy of ions striking the cathode could be up to several hundreds of eV higher than when striking the anode. In fact, optoelectronic quality hydrogenated amorphous silicon films are obtained in anodic conditions under soft ion bombardment, whereas the growth of diamondlike amorphous carbon films requires cathodic conditions under high ion bombardment. Although BN films have been deposited on substrates placed on both grounded and powered electrodes, to our knowledge no systematic study of the effect of the substrate electrode has been reported. In addition, despite the work done in characterizing the properties of BN films, relatively few reports deal with their stability when aging and exposed to atmosphere. Several stability studies have been reported for BN films obtained by thermal CVD,[19–21] but there is a lack of similar studies for PECVD BN films. Stability is crucial in determining the suitability of a thin-film material for application as a protective coating.

The present study investigates the preparation, properties, and stability of PECVD BN films obtained on both electrodes (anode and cathode) of a parallel-plate rf reactor by glow discharge decomposition of two different gas mixtures: B_2H_6–H_2–NH_3 and B_2H_6–N_2. This deposition technique is used worldwide in the semiconductor industry and the above gases are commonly employed, in combination with silane gas, for the preparation of silicon nitride and amorphous silicon-based devices. Thus, the findings of this study could also be of interest for the use of BN films in the fabrication of semiconductor devices. The properties of the BN films were analyzed by Fourier transform infrared (FTIR) spectroscopy, Raman spectroscopy, scanning electron microscopy (SEM), high-resolution transmission electron microscopy (HRTEM), x-ray photoelectron spectroscopy (XPS), and optical transmittance spectrophotometry in the visible–near-UV region.

II. EXPERIMENT

A. Film preparation

The deposition system consists of a capacitively coupled rf plasma reactor provided with a computer-controlled gas supply and vacuum system.[22] The reactor chamber is a cylindrical stainless-steel vacuum vessel 30 cm in diameter with two planar electrodes placed vertically and 4 cm apart. The substrate electrode (100 cm^2 in area) can be externally heated and connected either to ground or to an rf (13.56 MHz) generator via an automatic matching network. The gas mixtures used as source precursors were: (a) diborane (diluted to 1% of volume in hydrogen) plus ammonia, and (b) diborane (diluted to 5% of volume in nitrogen) plus nitrogen. These gases were admitted to the reaction chamber through separate gas lines and their flows regulated by mass flow controllers. After being mixed in a gas-blender box, the reacting gases flowed downstream along the interelectrode gap and were evacuated by pumping equipment consisting of turbomolecular, Roots, and rotary pumps. The total gas pressure was adjusted by a throttle valve and measured by an absolute capacitance manometer. Several kinds of substrates (fused silica, Corning 7059 glass, crystalline silicon polished on one and both sides, and NiCr-coated silicon) were used in order to perform the different film analyses. Before deposition, the substrates were cleaned with acetone and methanol, blown dry with nitrogen, and heated at 300 °C in vacuum (10^{-4} Pa) for several hours.

TABLE I. Deposition conditions for the B_2H_6–H_2–NH_3 gas system.

Substrate position:	Anode	Cathode
rf power density (W/cm^2):	0.25–0.5	0.3–0.5
Gas pressure (Pa):	30, 60	20–60
B_2H_6(1% in H_2) flow (sccm):	50, 60, 100	50, 60
NH_3 flow (sccm):	2.5, 5	2.5, 5
B_2H_6/NH_3 flow ratio:	0.2, 0.4	0.1–0.4
Deposition rate (nm/min):	0.6–1.4	2–6

For this study, more than 30 rf discharges were run. The deposition conditions corresponding to each gas chemistry and substrate position (cathode or anode) are listed in Tables I and II. The range of deposition parameters explored was chosen to obtain transparent films of nearly stoichiometric composition. All the films were grown at a 300 °C substrate temperature. The film thicknesses, measured by a stylus profilometer and optical transmittance, ranged from 100 to 2000 nm.

B. Film characterization

Film surface morphology was studied using an Hitachi 2300 scanning electron microscope working at 15 kV acceleration voltage. Cross-sectional HRTEM and dark-field (DF) images as well as selected area diffraction (SAD) patterns were recorded using a Philips CM 30 transmission electron microscope operating at 300 kV.

The optical transmittance of films deposited on fused silica and Corning 7059 substrates was measured by a Shimazdu 2101 PC spectrometer in the 200–800 nm range. The infrared properties were studied with a DA3 Bomem FTIR spectrometer working within the 500–4000 cm^{-1} wave numbers with a resolution of 4 cm^{-1}. FTIR transmittance spectra were measured under vacuum conditions using a polished on both sides (100) silicon wafer (50% transmittance) as a reference. Micro-Raman measurements were performed in backscattering geometry with a Jobin Yvon T64000 triple-

TABLE II. Deposition conditions for the B_2H_6–N_2 gas system.

Substrate position:	Anode	Cathode
rf power density (W/cm^2):	0.5	0.5
Gas pressure (Pa):	10, 30	10
B_2H_6(5% in N_2) flow (sccm):	30	4–6, 20
N_2 flow (sccm):	0	0, 25
B_2H_6/N_2 flow ratio:	5×10^{-2}	7×10^{-3}–5×10^{-2}
Deposition rate (nm/min):	3–6	6–9, 25

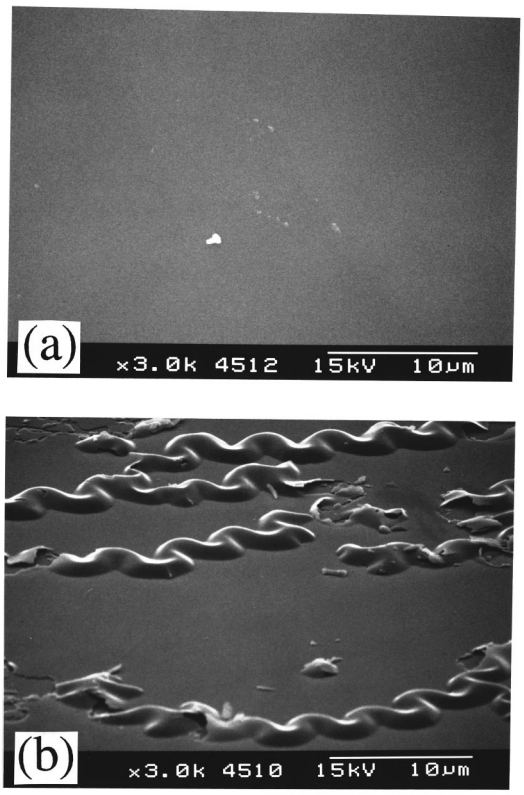

FIG. 1. SEM images of BN films deposited onto *c*-Si substrates placed on (a) the anode (130 nm thick) and (b) the cathode (110 nm thick), using the B_2H_6–H_2–NH_3 gas system.

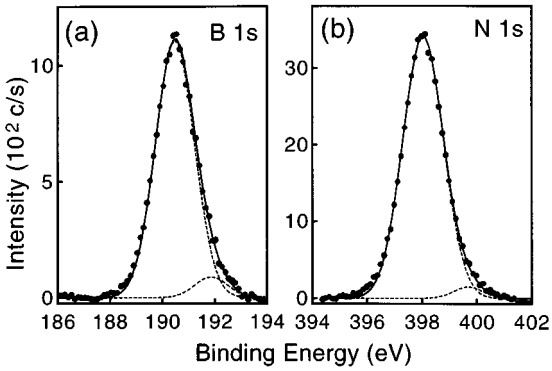

FIG. 2. Surface XPS spectra of (a) B 1*s* and (b) N 1*s* core levels of a BN film obtained from the B_2H_6–H_2–NH_3 gas mixture.

stage monochromator using the 488 nm line of an Ar laser as the excitation wavelength. The incident power density on the surface sample was 4 mW/μm^2.

XPS analysis was carried out with a Perkin–Elmer PHI 5500 spectrometer, using the $K\alpha$ line Al (1486.6 eV) as the x-ray source. The composition of the films (B/N atomic ratio) was calculated from the ratio between the total area of the XPS signals corresponding to the B(1*s*) and N(1*s*) core levels using the sensitivity factors of the instrument. This calculation was performed from signals measured without any argon etching of the film surface in order to avoid the effect of a greater sputtering yield of N atoms than of B atoms.[2] The C(1*s*) core level of adsorbed hydrocarbon at 285 eV was used as an energy calibration. XPS spectra of B1(*s*), N1(*s*), C(1*s*), and O(1*s*) were also recorded after sputtering the film surface with 3 kV argon ions.

III. RESULTS

A. B_2H_6–H_2–NH_3 gas mixture

1. Deposition rate, morphology, and composition of the BN films

With this gas system, transparent BN films were obtained on the anode at a deposition rate of about 1 nm/min, and on the cathode at a rate in the range of 2–6 nm/min. Figure 1 shows SEM images of BN films deposited on each electrode. Anodic films were smooth [Fig. 1(a)], adhered well to substrates, and were not scratched when abraded with stainless-steel tweezer tips. Microhardness measurements performed with a nanoindenter indicated values of around 15 GPa. The mass density calculated from x-ray reflection measurements was 1.95 g/cm^3. The average surface roughness determined with atomic force microscopy and real-time ellipsometry[23] was less than 1 nm. In contrast, SEM images of cathodic films reveal ridge-type buckling characteristic of high compressive stress [Fig. 1(b)]. These cathodic films were easily scratched and often became translucent and flaked or delaminated when exposed to atmosphere.

The chemical composition for both kinds of films was near stoichiometric as analyzed by XPS, with B/N atomic ratios between 1 and 1.1. Figures 2(a) and 2(b) show the surface XPS spectra corresponding to the B(1*s*) and N(1*s*) core levels, respectively, for a film deposited on the anode. Similar spectra were obtained for cathodic films. The deconvolution of the B1(*s*) signal gives two components: one intense at 190.5 eV (94% in area) corresponding to B linked to N, and another weaker at 191.9 eV ascribed to B–O bonds. The N(1*s*) signal shows a main peak at 398 eV (97% in area) characteristic of B–N bonding, and a small component at 399.7 eV possibly related to N–H bonds. After 2 min of Ar-ion etching of the film surface, no carbon signal was detected and the oxygen content was less than 4%. The film composition was homogeneous through the whole thickness as revealed by XPS depth profile analysis.

2. Optical and structural characterization

Films were highly transparent in the visible–near-UV range as shown in Fig. 3(a), where the optical transmittance spectrum of a BN film and of a fused silica substrate are plotted together. The refractive index measured by ellipsometry at a wavelength of 350 nm was around 1.80.[23] The absorption coefficient, α, in the near-UV region as a function of incident photon energy E is shown in Fig. 3(b). An optical band-gap energy of 5.6 eV was calculated from the x-axis intercept of the linear part of the plot $(\alpha E)^2$ versus E [Fig. 3(c)], corresponding to a direct allowed transition.

The FTIR spectra of the BN films grown on *c*-Si wafers (Fig. 4) showed two main absorption bands: one at around

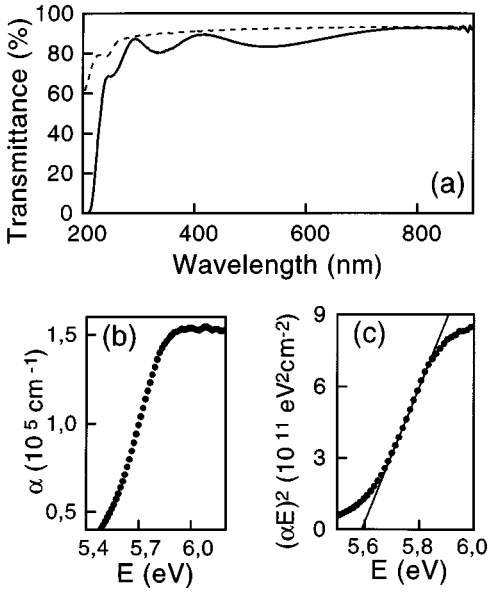

FIG. 3. (a) Optical transmittance spectrum of a 200 nm thick BN film (solid line) and of a fused silica substrate (dashed line). (b) Absorption coefficient α as a function of photon energy E. (c) Determination of optical gap energy from the plot of $(\alpha E)^2$ vs E.

1380 cm^{-1}, corresponding to the in-plane stretching B–N vibration mode (E_{1u}), and another at 780 cm^{-1} corresponding to the out-of-plane bending B–N mode (A_{2u}).[24] These TO vibrational modes are characteristic of the hexagonal phase of BN, and are the only excited modes in transmittance at normal incidence. The peak around 1380 cm^{-1} always exhibited a shoulder on the high wave-number side, which is attributed to the contribution of two-phonon processes.[24] In addition, the spectra showed a weak absorption band for the N–H stretching vibration (3435 cm^{-1}), whereas absorptions related to B–H bonds (2538 cm^{-1}) could hardly be seen.

Figure 5 shows the infrared absorption spectra of films

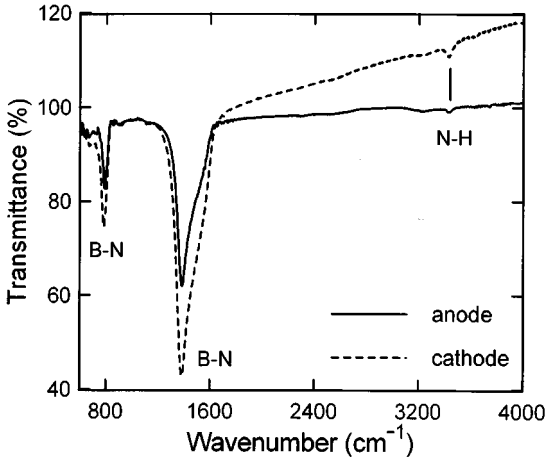

FIG. 4. FTIR transmittance spectra of BN films deposited on the anode (140 nm thick) and the cathode (220 nm thick), using the B_2H_6–H_2–NH_3 gas mixture.

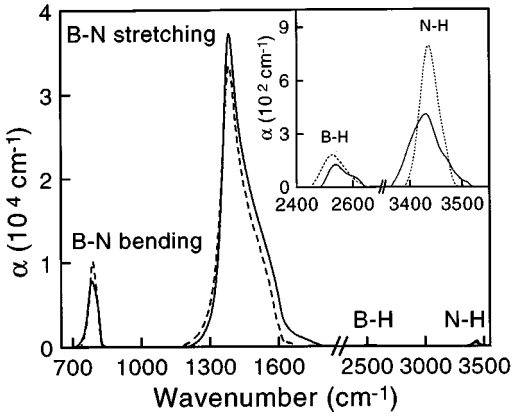

FIG. 5. Infrared absorption spectra of BN films grown on the cathode (solid line) and on the anode (dashed line) from B_2H_6–H_2–NH_3 gases.

deposited on the anode and on the cathode, which were calculated from the FTIR transmittance spectra and the film thicknesses. It can be seen that the absorption band of the B–N stretching mode is more intense for cathodic samples, whereas that of the B–N bending mode is more intense for anodic films. As the optical properties of *h*-BN are anisotropic, the ratio of the heights of the BN stretching and bending peaks depend on the orientation of the BN basal planes against the substrate surface and, under optical normal incidence, becomes minimal when the *c*-axis is parallel to the substrate plane. Therefore, this could indicate a preference in texture of the anodic films over the cathodic ones. In fact, IR reflection spectra performed with polarized light at several incidence angles revealed the presence of the LO component of the stretching mode and the absence of the LO component of the bending mode. This indicated that the principal *c* axis of *h*-BN planes lay within the plane parallel to the film surface but was randomly oriented.[25]

From the integrated absorption intensity corresponding to N–H and B–H stretching modes (Fig. 5) and using calibration constants reported for these modes,[26,27] an atomic content of hydrogen, mostly bonded to nitrogen, of about 7% for films grown on the anode and between 5% and 15% for films grown in the cathode, depending on deposition conditions, was calculated.

The Raman spectra of the films exhibited the high-frequency E_{2g} vibration mode characteristic of *h*-BN.[24] Some differences in both position (ω) and at full width at half maximum (FWHM) of the peak were observed between anodic and cathodic films. Typical values for anodic films were 1373 cm^{-1} (ω) and 60 cm^{-1} (FWHM), whereas they were 1368 cm^{-1} and 40 cm^{-1} for cathodic ones. These results were independent of the kind of substrate used, as shown in Fig. 6. According to the study by Nemanich *et al.*,[28] our films are thought to have a nanocrystalline structure with crystallite sizes of around 3 and 5 nm for anodic and cathodic films, respectively.

The nanocrystallinity and the preferred texture of the films were confirmed by cross-sectional and SAD observations. A textured microstructure was observed throughout the

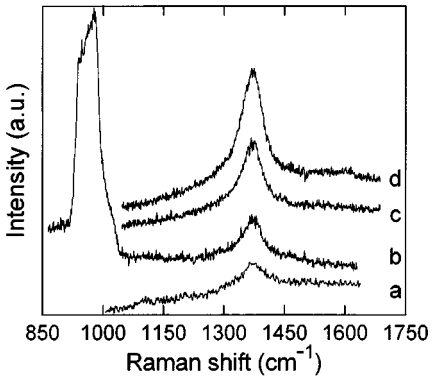

FIG. 6. Raman spectra of BN films grown on several substrates: (a) Corning glass, (b) silicon, (c) WC–Co, and (d) Ni–Cr-coated silicon.

whole thickness of the BN films grown on the anode, showing *h*-BN lattice fringes aligned nearly perpendicular to the substrate with an interplanar distance of about 0.35 nm (Fig. 7). The SAD pattern showed two bright arcs, indexed as (002) reflections of *h*-BN, along with continuous rings corresponding to (100) and (110) *h*-BN reflections. The preferred orientation is corroborated in the DF image of Fig. 8(a), where bright areas denote the textured *h*-BN nanocrystallites contributing to (002) reflection. Such contrast is not observed in the DF image of Fig. 8(b), obtained from the dark part of the (002) *h*-BN ring. On the contrary, cross-sectional HRTEM analysis of films grown on the cathode showed a layered microstructure,[29] which was composed of an initial *a*-BN layer next to the substrate followed by a *h*-BN textured layer with its *c* axis parallel to the substrate surface, and another *h*-BN layer oriented at random.

FIG. 7. Cross-sectional HRTEM image and SAD pattern of a 190 nm thick BN film grown on the anode using the B_2H_6–H_2–NH_3 mixture.

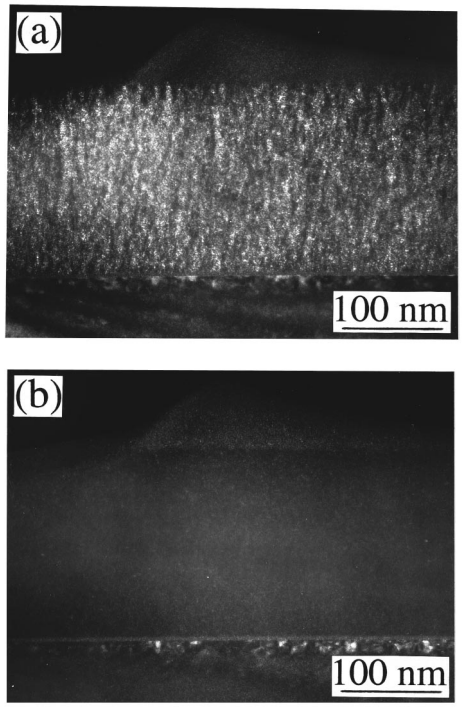

FIG. 8. TEM dark-field images of film shown in Fig. 7. Bright areas in each picture show the (002) *h*-BN planes (a) perpendicular and (b) parallel to the Si substrate surface.

3. Film stability

The stability of the films after long-time exposition to humid atmosphere was monitored by FTIR analysis. Cathodic films degenerated with aging, which led to a slight reduction of the B–N bands in the IR spectra along with the appearance of absorption peaks at 2854, 2925, and 2956 cm^{-1} related to C–H_n groups (Fig. 9). In addition, their optical transmittance decreased [Fig. 10(a)] and the XPS analysis confirmed a large increase of carbon atoms (up to

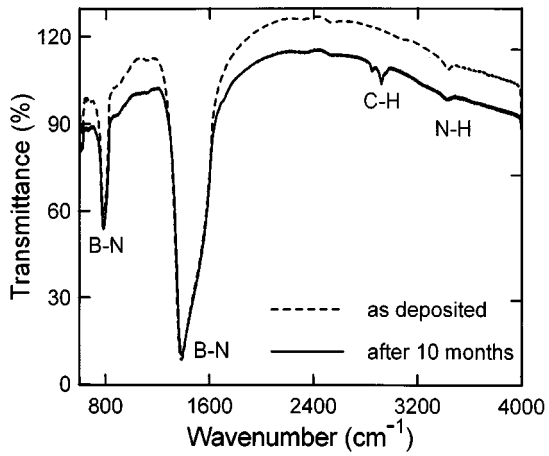

FIG. 9. Evolution of the FTIR transmittance spectrum of a 600 nm thick cathodic BN film, deposited on silicon from the B_2H_6–H_2–NH_3 mixture, after ten months of air exposition.

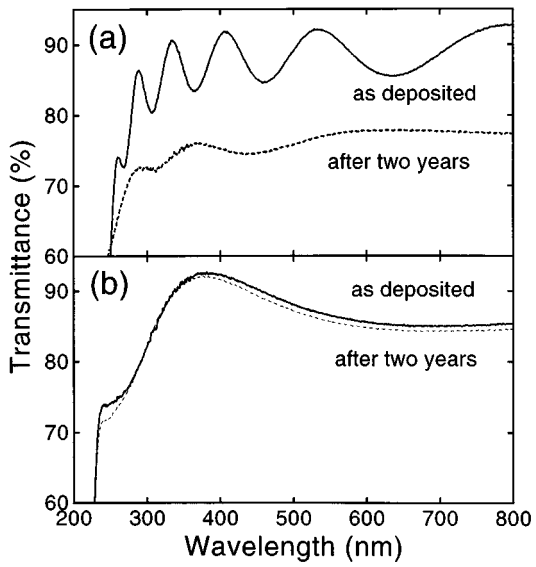

FIG. 10. Evolution of the optical transmittance of BN films of the B_2H_6–H_2–NH_3 gas system deposited (a) on the cathode and (b) on the anode. The film spectra were taken as deposited (solid line) and after two years of air exposition (dashed line).

15%) in the degraded films with no significant changes in the relative percentages of B, N, and O contents.

In contrast, the BN films grown on the anode were chemically and physically very stable and showed identical infrared and optical transmittance spectra [Fig. 10(b)], even after aging periods as long as two years.

B. B_2H_6–N_2 gas mixture

1. Deposition rate, morphology, and composition of the BN films

BN films were first deposited using the diborane (5% in nitrogen) mixture without further N_2 dilution. On the anode, white and hazy films, easily scratched with a blade, grew at a rate of 6 nm/min. A typical SEM image of these films, shown in Fig. 11(a), reveals a mosaic morphology indicative of high tensile stress. In contrast, well-adhered, unscratched films were obtained on the cathode at a growth rate of 25 nm/min. These films were brown in color and had B/N atomic ratios of 1.5 measured by XPS. Adding nitrogen to achieve relative B_2H_6/N_2 flow percentages in the 0.7%–1% range, transparent and near-stoichiometric ($0.95<\mathrm{B/N}<1.1$) films were deposited on the cathode at a rate between 6 and 9 nm/min. The surface of these cathodic films was smooth, as the SEM image of Fig. 11(b) shows.

Surface XPS analysis of the stoichiometric BN films performed without Ar-ion etching showed that the main contribution to the N(1*s*) peak corresponded to nitrogen linked to boron at a binding energy of 398.1 eV. In addition, a weak contribution possibly from N–H bonds appeared at 399.9 eV. Boron was mainly bonded to nitrogen at a binding energy of 190.6 eV, but the B(1*s*) peak also showed a weak contribution at 192.2 eV ascribed to B–O bonding. No carbon signal was observed in the XPS spectra performed after 2 min surface Ar-ion etching; the oxygen atomic concentration was less than 2%.

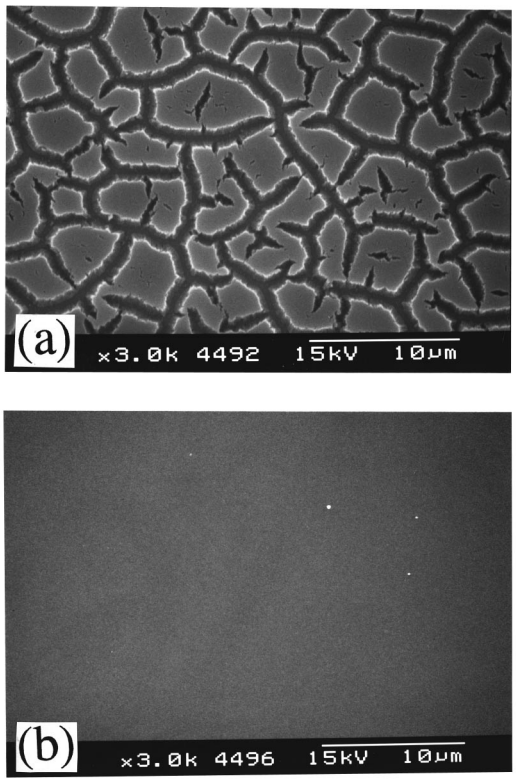

FIG. 11. SEM images of BN films deposited on silicon substrates placed (a) on the anode (675 nm thick) and (b) on the cathode (675 nm thick) from the B_2H_6–N_2 gas mixture.

2. Optical and structural characterization

The films were as highly transparent in the visible–near-UV range as the films obtained from the B_2H_6–H_2–NH_3 mixture. However, the absorption edge was slightly shifted to larger wavelengths, resulting in optical band-gap energies around 4.9 eV. The main features of the FTIR spectra (Fig. 12) were the absorptions related to the B–N modes along with a weaker band corresponding to the N–H stretching mode. The anodic films spectra showed additional bands at around 920 and 2520 cm^{-1}, ascribed to B–H bending and stretching modes, respectively, which could barely be seen in the cathodic films spectra. The infrared absorption spectrum of a film grown on the cathode is shown in Fig. 13. The absorption band of the B–N stretching mode is wider and its intensity lower than the absorption band of the anodic films prepared from the B_2H_6–H_2–NH_3 mixture. In addition, the B–N bending absorption band is slightly shifted at lower wavelengths. The estimated hydrogen atomic content, mostly linked to N atoms, was around 10%.

The same textured polycrystalline *h*-BN structure found in the anodic films using the B_2H_6–H_2–NH_3 mixture was confirmed by cross-sectional TEM analysis of cathodic films prepared from B_2H_6–N_2 gases. SAD patterns [(Fig. 14(a)]

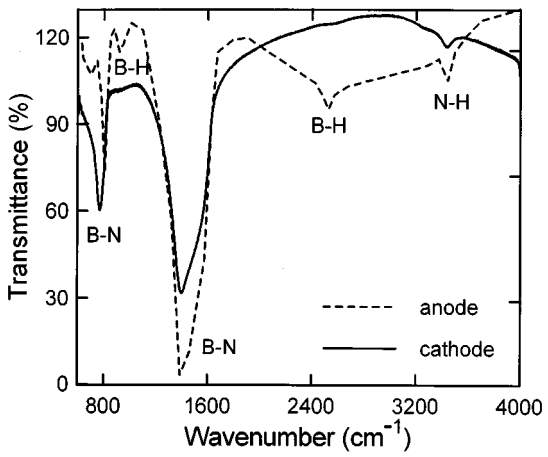

FIG. 12. FTIR transmittance spectra of BN films obtained from the B_2H_6–N_2 gas system and deposited on the anode (675 nm thick) and on the cathode (575 nm thick).

showed two arcs indexed as (002) reflection of *h*-BN, along with continuous rings ascribed to (100) and (001) reflections of *h*-BN. DF images obtained using the beams diffracted towards the bright arcs and towards the dark part of the (002) *h*-BN ring, are shown in Figs. 14(b) and 14(c), respectively, corroborating that the *c* axis was in the plane parallel to the film surface.

3. Film stability

Cathodic films from the B_2H_6–N_2 mixture were very stable and their infrared and optical transmittance spectra remained unchanged after several months of being exposed to atmosphere. On the contrary, the films obtained on the anode quickly became degraded, as comparison between the infrared spectra taken the same day of deposition and after 15 days of air exposure showed (Fig. 15). The intensities of B–N bands were strongly lowered, the B–H stretching band disappeared, and a wide absorption band related to O–H groups was developed in the 3000–3500 cm^{-1} region. After eight months of air exposure, the FTIR spectra showed the

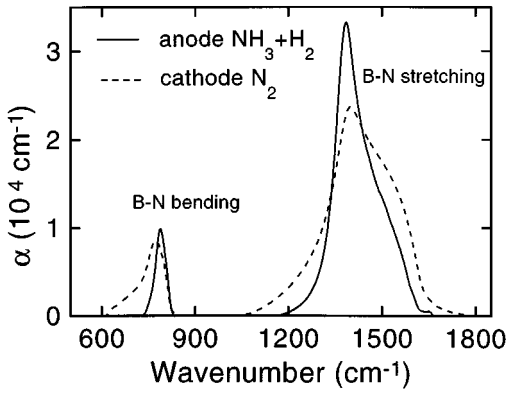

FIG. 13. Infrared absorption spectra of stable and adherent BN films deposited on the cathode from B_2H_6–N_2 gases (dashed line) and on the anode using the B_2H_6–H_2–NH_3 gas mixture (solid line).

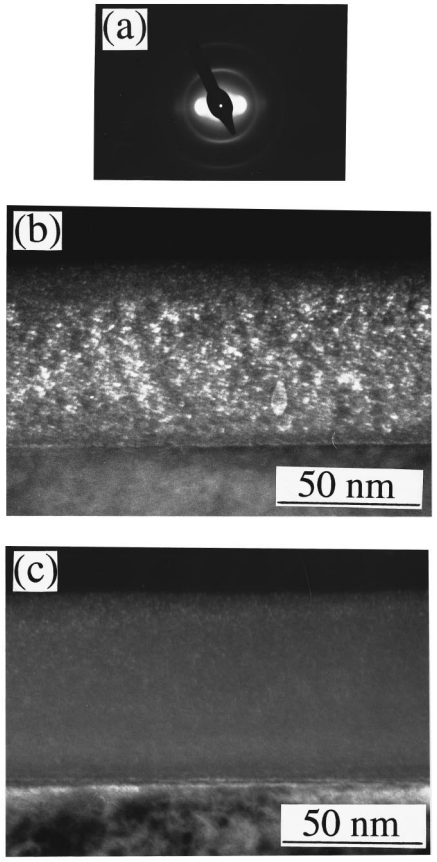

FIG. 14. SAD pattern (a) and dark-field images of a BN film grown on the cathode using the B_2H_6–N_2 mixture showing the (002) *h*-BN planes perpendicular (b) and parallel (c) to the Si substrate surface.

presence of several absorption peaks in the 900–1200 cm^{-1} region. In addition, XPS analysis indicated a loss of nitrogen atoms (B/N = 1.6) and the incorporation of oxygen (10%) and carbon atoms (18%). SEM images revealed the growth

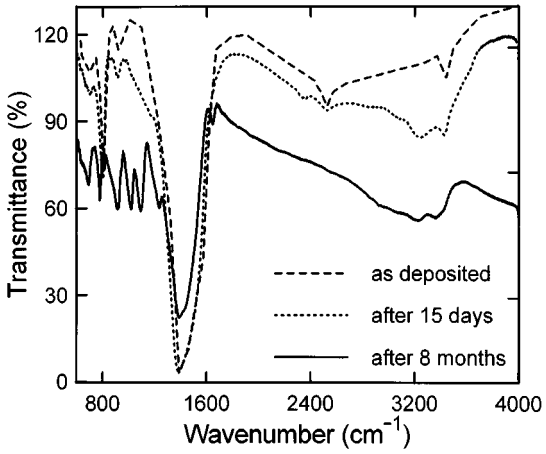

FIG. 15. Evolution of the FTIR transmittance of an unstable 700 nm thick BN film grown on the anode using the B_2H_6–N_2 gas system. The spectra were measured as deposited (dashed line) and after air exposition periods of 15 days (dotted line) and eight months (solid line).

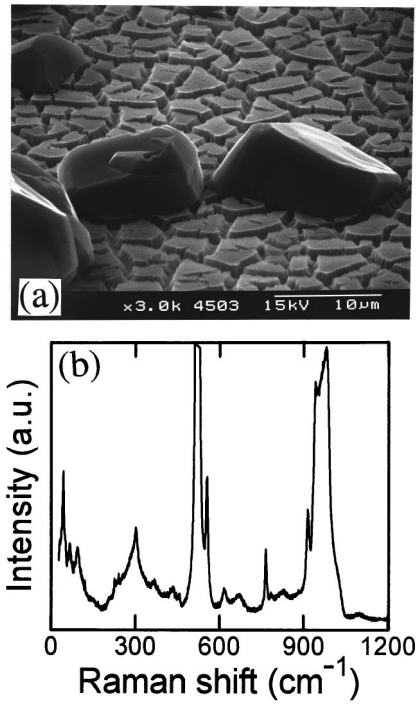

FIG. 16. (a) SEM image of the surface of an anodic unstable BN film obtained from B_2H_6–N_2–gases; (b) Micro-Raman spectrum of the crystals observed on the surface of unstable films and identified as ammonium borate hydrates (peaks at 520 and 960 cm^{-1} correspond to the silicon substrate).

of crystallites of about 10μm on the surface of the degraded films [Fig. 16(a)]. These crystals were analyzed by Raman [Fig. 16(b)] and identified as ammonium borate hydrates.[19]

IV. DISCUSSION

The above results indicated that PECVD BN films show different properties and stability behavior depending on the gas precursors used and the choice of anode or cathode for the substrate position. In particular, it has been found that some deposition conditions lead to adherent, textured *h*-BN films that are very stable upon exposure to air; whereas other conditions give rise to excessive stress in the films, either tensile or compressive, which often results in catastrophic failure and degradation of the films when exposed to atmosphere. These results will now be discussed in detail, examining the origin of film stress and the effects of ion bombardment on the growing films.

Intrinsic stress in thin films can arise from chemical, microstructural, and particle bombardment effects.[30] Chemical reactions taking place beneath the growth surface can promote compressive stress if they add material to the film structure, whereas those that remove material produce tensile stress. Energetic particle bombardment of the growing film surface creates compressive stress by transfer of momentum to surface atoms, forcing the atoms into closer proximity. As stated earlier, ion bombardment affects more the growth of cathodic films than of anodic ones, due to the negative self-bias voltage developed at the powered electrode (of around -200 V in our experiments). Ion bombardment on a growing film can have either beneficial or detrimental consequences on the film quality. The beneficial effects include the increased surface mobility of adsorbed radical reactive species, which helps to grow a dense material, the reduction of tensile stress produced by chemical or microstructural effects, and the removal of adsorbed contaminants and loosely adherent species from the film surface. However, intensive ion bombardment can damage the growing film by introducing excessive compressive strains, breaking bonds, creating defects, sputtering off radicals, and incorporating impurities.

The comparison of the properties and the deposition rate of BN films obtained on the anode from the two gas mixtures used suggests that different growth mechanisms occur depending on the precursor gases. For the B_2H_6–H_2–NH_3 mixture, the reaction of diborane and ammonia causes the formation of intermediate gas-phase compounds such as borazine ($B_3N_3H_6$), which leads to polymeric $(BNH_2)_n$ and $(BNH)_n$ precursor species.[31] When N_2 is used instead of NH_3, the BN film formation may occur through the direct reaction of N atoms and BH_n radicals that stick to the growing surface. The liberation of hydrogen linked to these radicals along with their probably high sticking coefficient could account for the observed tensile stress, and thus, the presence of cavities and voids in the anodic films. High internal porosity with unsaturated B–N bonds favors the hydrolysis of BN by moisture and could explain the degradation of films through the formation of ammonium borate hydrate crystals, as previously reported for unstable thermal CVD BN films.[19,20] Nevertheless, when the films are deposited on the cathode using the B_2H_6–N_2 mixture, the tensile stress and the low surface mobility of adsorbed species might be counteracted by the beneficial effects of ion bombardment, favoring the growth of dense, adherent, and stable films. On the contrary, the damaging effect of ion bombardment through excessive compressive stress is reflected in the deposition of cathodic films from the B_2H_6–H_2–NH_3 mixture.

One of the main findings of this study is that adherent, hard, and stable BN films are obtained with a *h*-BN structure where the *c* axis is parallel to the substrate surface, which differs from the usual *h*-BN structure observed in CVD films where the *c* axis is perpendicular to the substrate plane.[3] This preferred *h*-BN texture for the films deposited on the cathode using B_2H_6–N_2 gases can be explained as a result of the increasing biaxial compressive stress in the films induced by ion bombardment.[32] It should be noted that the formation of an intermediate *h*-BN layer with the same texturing is considered an essential condition for the nucleation of the *c*-BN phase.[7] Nevertheless, as for the films deposited on the anode from B_2H_6–H_2–NH_3 gases, the preferred *h*-BN texture is achieved under soft ion bombardment conditions, since the energy of incident ions should be only a few tenths of eV, the same as the plasma potential. One possible reason for this might be due to surface chemical changes caused by H atoms present in the hydrogen-rich B_2H_6–H_2–NH_3 discharge, such as the increased surface mobility of adsorbed species or a selective chemical etching, which favor the *h*-BN growth with the *c* axis parallel to the substrate surface. As a matter

of fact, the same textured growth has been reported for sputtered aluminum nitride films in a gas mixture containing H_2, whereas without the presence of hydrogen the films grew with the *c* axis at a normal angle to the substrate.[33] Finally, the present authors recently reported the successful growth of high-quality polycrystalline continuous diamond films by hot-filament CVD onto these textured *h*-BN films,[34] which opens up the possibility of growing multilayered structures for mechanical coatings and electronic applications based on the diamond–BN system.

V. CONCLUSIONS

For a given PECVD system, the properties of BN films are strongly dependent on both the gas chemistry used and the choice of anode or cathode for the substrate electrode. Further, the feasibility of obtaining hard and transparent *h*-BN films with a prefered texture in a low-temperature plasma process has been shown. The interesting properties and high stability of these textured BN films make them useful for applications in the fields of ceramic coatings and microelectronic devices.

ACKNOWLEDGMENTS

This work was partially supported by the CICYT of Spain under Contract Nos. MAT93-0298 and MAT96-0552. The authors acknowledge the Serveis Científico–Tècnics of the Universitat de Barcelona for their film characterization facilities.

[1]*Properties of Group III Nitrides*, edited by J. H. Edgard (INSPEC, London, 1994).
[2]L. B. Hackenberger, L. J. Pilione, and R. Messier, in *Science and Technology of Thin Films*, edited by F. C. Mattacotta and G. Ottaviani (World Scientific, Singapore, 1995), p. 121.
[3]R. T. Paine and C. K. Narula, Chem. Rev. **90**, 73 (1990).
[4]S. P. S. Arya and A. D'Amico, Thin Solid Films **157**, 267 (1988).
[5]D. R. Cote, S. V. Nguyen, W. J. Cote, S. L. Pennington, A. K. Stamper, and D. V. Podlesnik, IBM J. Res. Dev. **39**, 437 (1995).
[6]*Synthesis and Properties of Boron Nitride*, edited by J. J. Pouch and S. A. Alterovitz (Trans. Tech., Zürich, 1990).
[7]T. Yoshida, Diamond Relat. Mater. **5**, 501 (1996).
[8]D. J. Kester, K. S. Ailey, D. J. Lichtenwainer, and R. F. Davis, J. Vac. Sci. Technol. A **12**, 3074 (1994).
[9]O. Tsuda, Y. Yamada, T. Fujii, and T. Yoshida, J. Vac. Sci. Technol. A **13**, 2483 (1995).
[10]D. L. Medlin, T. A. Friedman, P. B. Mirkarimi, M. J. Mills, and K. F. McCarty, J. Appl. Phys. **76**, 295 (1994).
[11]T. H. Yuzuhira and D. W. Hess, Thin Solid Films **140**, 199 (1986).
[12]S. V. Nguyen, T. Nguyen, H. Treichel, and O. Spindler, J. Electrochem. Soc. **141**, 1633 (1994).
[13]E. H. A. Dekempeneer, J. Meneve, S. Kuypers, and J. Smeets, Surf. Coat. Technol. **74-75**, 399 (1995).
[14]C. Schaffnit, H. Del Puppo, R. Hugón, L. Thomas, P. Moretto, F. Rossi, and Y. Pauleau, Surf. Coat. Technol. **80**, 13 (1996).
[15]R. Zedlitz, M. Heintze, and M. B. Schubert, J. Non-Cryst. Solids **198-200**, 403 (1996).
[16]W. Dworschak, K. Jung, and H. Ehrhardt, Thin Solid Films **254**, 65 (1995).
[17]T. Ichiki, T. Momose, and T. Yoshida, J. Appl. Phys. **75**, 1330 (1994).
[18]Y. Osaka, A. Chayahara, H. Yokohama, M. Okamoto, T. Hamada, T. Imura, and M. Fujisawa, Mater. Sci. Forum **54-55**, 277 (1990).
[19]T. Matsuda, J. Mater. Sci. **24**, 2353 (1989).
[20]V. Cholet, L. Vandenbulcke, J. P. Rouan, P. Baillif, and R. Erre, J. Mater. Sci. **29**, 1417 (1994).
[21]C. Gómez-Aleixandre, A. Essafti, M. Fernández, J. L. G. Fierro, and J. M. Albella, J. Phys. Chem. **100**, 2148 (1996).
[22]J. L. Andújar, E. Bertran, A. Canillas, C. Roch, and J. L. Morenza, J. Vac. Sci. Technol. A **9**, 2216 (1991).
[23]E. Bertran, A. Canillas, M. El Kasmi, E. Pascual, J. Costa, and J. L. Andújar, Mater. Res. Soc. Symp. Proc. **410**, 307 (1996).
[24]R. Geick, C. H. Perry, and G. Rupprecht, Phys. Rev. **146**, 543 (1966).
[25]M. C. Polo, M. Ben el Mekki, J. L. Andújar, N. Mestres, and J. Pascual, Diamond Relat. Mater. **6**, 1550 (1997).
[26]W. A. Lanford and M. J. Rand, J. Appl. Phys. **49**, 2473 (1978).
[27]K. Shirai and S. Gonda, J. Appl. Phys. **67**, 6286 (1990).
[28]R. J. Nemanich, S. A. Solin, and R. M. Martin, Phys. Rev. B **23**, 6348 (1981).
[29]J. L. Andújar, E. Bertran, and Y. Maniette, J. Appl. Phys. **80**, 6553 (1996).
[30]D. L. Smith, *Thin Film Deposition: Principles and Practice* (McGraw-Hill, New York, 1995).
[31]M. J. Rand and J. F. Roberts, J. Electrochem. Soc. **115**, 423 (1968).
[32]D. R. McKenzey, W. D. McFall, W. G. Sainty, C. A. Davis, and R. E. Collins, Diamond Relat. Mater. **2**, 970 (1993).
[33]H.-C. Lee, K.-Y. Lee, Y.-J. Yong, J.-Y. Lee, and G.-H. Kim, Thin Solid Films **271**, 50 (1996).
[34]M. C. Polo, G. Sánchez, W. L. Wang, J. Esteve, and J. L. Andújar, Appl. Phys. Lett. **70**, 1682 (1997).